

Dimitry Papkov¹

Department of Mechanical and
Materials Engineering,
Nebraska Center for Materials and Nanoscience,
University of Nebraska-Lincoln,
Lincoln, NE 68588-0526
e-mail: dpapkov@huskers.unl.edu

Alexander Goponenko

Department of Mechanical and
Materials Engineering,
Nebraska Center for Materials and Nanoscience,
University of Nebraska-Lincoln,
Lincoln, NE 68588-0526

Owen C. Compton²

Department of Chemistry,
Northwestern University,
Evanston, IL 60208

Zhi An

Department of Chemistry,
Northwestern University,
Evanston, IL 60208

SonBinh T. Nguyen

Department of Chemistry,
Northwestern University,
Evanston, IL 60208

Yuris A. Dzenis

Department of Mechanical and
Materials Engineering,
Nebraska Center for Materials and Nanoscience,
University of Nebraska-Lincoln,
Lincoln, NE 68588-0526

Controlled Nanofabrication of Uniform Continuous Graphene Oxide/Polyacrylonitrile Nanofibers for Templated Carbonization

Graphene and graphene oxide attract rapidly growing interest as prospective building blocks for nanotechnology applications and composites. Recently, we showed that a small amount of graphene oxide produced significant templating effects on the structure of continuous carbon nanofibers (CNFs). However, the produced nanofibers had significant nonuniformities that could be detrimental to their mechanical properties. Controlled nanofabrication is critical for obtaining uniform, high-quality nanofibers with tunable diameters and properties. Here, we analyze the effects of graphene oxide type, concentration, and processing parameters on the morphology of continuous graphene oxide/polyacrylonitrile nanofibers produced by electrospinning. Four types of graphene oxides with different average nanoparticle sizes were examined, and the effects of electric field and polymer concentration on nanofiber diameters were analyzed. Good-quality nanofibers were produced with up to 2 wt % graphene oxide in polyacrylonitrile. Uniform nanofibers were obtained for solid content above 9 wt % in dimethylformamide (DMF). Composite nanofibers containing graphene oxide nanoparticles exhibited reduced diameters throughout the polyacrylonitrile concentration range before and after carbonization compared to nanofibers prepared from neat polymer. The obtained results open up a pathway for controlled nanofabrication of uniform CNFs with improved structure for a variety of structural and functional applications. [DOI: 10.1115/1.4045211]

Keywords: electrospinning, poly (acrylonitrile), continuous nanofibers, graphene oxide, nanofiber diameter, carbonization templating

Introduction

Nanocarbons with unique chemical, electronic, and mechanical characteristics represent attractive building blocks for novel functional materials and devices [1]. To date, carbon nanotubes (CNTs) have been most extensively studied; however, graphene and graphene oxide gain steadily growing interest, as fully exfoliated and stable graphene and graphene oxide can now be produced by several methods inexpensively [2]. Graphene and graphene oxide possess properties that rival those of carbon nanotubes and have large surface areas that can be functionalized to interact strongly with a range of materials and environments. Graphene particles have been incorporated in polymer nanocomposites [3–7] and shown to produce considerable mechanical improvements at small particle loadings [4,7]. These improvements have been attributed to strong interactions between the polymers and nanoparticles. Evidence of these interactions can be seen in dramatic increases in polymer glass transition temperatures (T_g) [4,7]. However, the low-volume-fraction polymer nanocomposites, while being attractive for functional applications, cannot yet replace existing high-performance structural composites, such as carbon-epoxy. Recently, attempts have been made to produce high-strength neat graphene and graphene oxide fibers

[8–12]. The mechanical performance of these early fibers so far fell short of the performance of existing advanced fibers, but the results show promise. Nevertheless, if recent history of CNT fibers is any guide, development of high-volume-fraction, ultrahigh-performance graphene or graphene oxide fibers and composites may take considerable time and effort.

Recently, an alternative strategy to utilize unique graphene oxide structure and properties in high mechanical performance materials was proposed and implemented [13]. This method did not rely on graphene oxide particles as reinforcement. Rather, a small amount of nanoparticles was used to serve as a templating agent to improve the structure of carbon fibers during carbonization. Significant improvements in graphitic structure quality and, notably, preferred orientation were demonstrated in carbon nanofibers (CNFs) produced by carbonization of electrospun polyacrylonitrile (PAN) precursors. A large reduction in polymer crystallinity was observed as a result of addition of a small amount (1.4 wt %) of graphene oxide by examining the X-ray spectra of the precursor nanofibers. After carbonization, significant improvements in graphitic structure were observed by examining Raman spectra of the CNFs. Smaller D/G band intensity ratios and narrower G band indicated larger nanocrystal size and better graphitic structure. Improved crystal orientation in CNFs was observed by selected area electron diffraction (SAED).

Unlike the bottom-up synthetic growth processes, the top-down electrospinning nanomanufacturing produces continuous nanofibers (NFs) [14]. These NFs are much easier and safer to handle and process into applications and composites. NFs from appropriate precursor polymers can then be carbonized to produce CNFs. Continuous CNFs with improved graphitic structure achieved at

¹Corresponding author.

²Present address: E. I. DuPont de Nemours and Company, Inc., Central Research & Development, Experimental Station, Wilmington, DE 19880

Contributed by the Manufacturing Engineering Division of ASME for publication in the JOURNAL OF MICRO- AND NANO-MANUFACTURING. Manuscript received February 25, 2019; final manuscript received October 1, 2019; published online November 14, 2019. Assoc. Editor: Shih-Chi Chen.

lower carbonization temperatures [13,15] can lead to inexpensive strong fibers and structural nanocomposites [13,15]. The key to realizing this will be controllable production of graphene oxide-modified nanofiber precursors. Electrospinning is a complex multiphysics process [14] that will be affected by the addition of irregularly shaped, conductive graphene-oxide nanoparticles. In general, smaller nanoparticles at lower volume fractions can be expected to produce more uniform nanofibers, but other process parameters such as electric field and polymer concentration in solution will affect the outcome. In addition, larger graphene oxide nanoparticles might be more beneficial for “anchoring” polymer chains during stabilization and carbonization, as discussed in Ref. [13]. While optimal nanoparticle volume fraction for the carbonization templating is not currently known, higher nanoparticle loadings might be beneficial for more uniform distribution of the templating nuclei within the nanofibers. The resulting diameter of the templated nanofibers is also of critical importance as it significantly affects nanofiber mechanical properties and serves as an important scale parameter for nanostructured materials and devices.

The objective of this paper was to study the effects of graphene oxide nanoparticle type, size, concentration, and electrospinning processing parameters on the morphology of the resulting nanocomposite nanofibers with special emphasis on nanofiber diameter. In future studies, these results can be correlated with observed mechanical properties. The results will guide nanofabrication of novel graphene oxide-templated nanofibers with tunable diameters for structural and functional applications.

Experimental

Preparation of Graphene Oxide Nanoparticles. Graphite oxide (GO) was synthesized from graphite powder following a modified Hummers method [16]. In a 100-mL round-bottom flask equipped with a large Teflon-coated magnetic stir bar, graphite powder (5 g) was first pre-oxidized by vigorously stirring at 80 °C for 6 h in a mixture of H₂SO₄ (15 mL), K₂S₂O₈ (10 g), and P₂O₅ (10 g). The pre-oxidized powder was filtered and washed with ultrapure de-ionized water (3 × 50 mL) and dried at 50 °C overnight.

A 500-mL round-bottom flask was loaded with a large Teflon-coated magnetic stir bar, the pre-oxidized graphite, sodium nitrate (3 g), and sulfuric acid (150 mL) and then stirred vigorously to combine. After the sodium nitrate was dissolved, the flask was cooled down in an ice bath. While stirring, potassium permanganate (18 g) was added slowly over 10 min to prevent dangerous overheating (>20 °C), resulting in a green suspension almost instantaneously. The ice bath was replaced with a water bath, which was heated to 35 °C while the solution was stirred over 48 h. During this time, the solution became highly viscous and turned dark brown. The reaction flask was then cooled down in an ice/salt bath and ultrapure de-ionized water (230 mL) was slowly added to the solution, ensuring that the temperature remained below 40 °C. This resulted in a diluted muddy-colored mixture, which was quenched with aqueous 30 wt % hydrogen peroxide (12 mL), yielding a light yellow suspension of graphite oxide. The resulting graphite oxide was washed by three cycles of centrifugation (8230 g for 5 min), decantation, and resuspension in ultrapure de-ionized water (30 mL). Then it was washed with aqueous HCl (30 mL of a 1:9 v/v dilution of concentrated aqueous HCl) to remove residual metal cations, followed by five additional cycles of centrifugation/decantation/resuspension with ultrapure de-ionized water (30 mL).

Exfoliation into single-layer graphene oxide sheets was achieved by sonicating an aqueous suspension of graphite oxide (250 mL of a 10 mg mL⁻¹ solution) for 30 min in a laboratory bath sonicator (Fisher Scientific FS60). Un-exfoliated aggregates were removed from solution via centrifugation at 8000 rpm for 15 min, with the supernatant reserved. Dialysis of the supernatant

in ultrapure de-ionized water (4 × 2 L over a period of 2 days) was performed to remove any residual metal ions from the aqueous dispersion. Complete exfoliation was confirmed by the absence of a diffraction peak in the PXRD pattern of a freeze-dried aliquot of the dispersion. Elemental analysis (C, 45.23%; H, 2.36%; N, 0%; O, 47.64%) affords a C/O mole ratio of 1.27.

Nanofabrication. The nanomanufacturing process followed the protocols described in Ref. [13]. NFs were electrospun from a range of 7.5–12 wt % PAN (Pfaltz and Bauer, Inc.; MW 150,000) in dimethylformamide (DMF) (Sigma-Aldrich), at a range of operating voltages 4–18 kV, from a 10–20-cm spinneret–collector distance, using a 0.6 ml/h feed rate, and a 20 ga needle. In case of graphene oxide-modified NFs, the corresponding amount of graphene oxide was added. The solution was sonicated in an ultrasonic bath until a uniform dispersion was achieved prior to electrospinning.

X-Ray Structural Analysis. NF crystallinity was evaluated following protocols from Ref. [13]. Nanofiber mats were electrospun for structural analysis onto an aluminum substrate. Wide-angle X-ray diffraction (XRD) analysis was performed using a Rigaku Multiflex X-ray diffractometer with Cu K α radiation in the range of 2θ between 10 deg and 50 deg. The background was removed, and the crystalline peak (or peaks in the case of annealed samples) and the amorphous halo were fitted using Lorentzian peak shapes.

Results and Discussion. Papkov et al. [13] examined the effect of single type of graphene oxide, size, and concentration on NF structure. Changes in these parameters, together with changes in process parameters, can have a significant impact on NF morphology and structure. In order to examine the effect of these changes, several types of graphene oxide particles were prepared.

Preparation of Different Graphene Oxide Nanoparticles. In order to produce different sizes of graphene oxide particles, additional high-power sonication to reduce the size of graphene oxide sheets was performed using a probe ultrasonicator (Vibra-Cell™ VC 505 (500 W), Sonics & Materials, Inc., Newtown, CT) set at 30% intensity, 10 s/10 s pulse, for variable periods of ON time (graphene oxide sonicated for 1, 2, and 4 h will be designated as GO-A, GO-B, and GO-C, respectively). In case of graphene oxide that will be designated as GO-nano, smaller initial particle size graphite powder was used, and no additional sonication was performed after the exfoliation process.

Particle size distribution for the different types of graphene oxide, as measured by dynamic light scattering (DLS) technique, can be seen in Fig. 1. It should be noted that DLS measurements model particle size as spheres, which is not true for graphene oxide sheets, and hence the particle size in the charts cannot be taken as the true particle size. The average DLS-derived particle sizes for GO-A, GO-B, GO-C, and GO-nano were 465, 350, 206, and 227 nm, respectively. It should be noted that the average values are based on Z-average provided by the instrument software and are skewed due to the presence of large particles.

As can be seen from the figure, there is a significant statistical variation between the different test runs, which is especially apparent for the sonicated particles. The distributions indicate the presence of relatively large particles even when the average particle size is small, which could impact the quality of electrospun nanofibers.

Effect of Graphene Oxide Type on Nanofiber Morphology. As a first step, effect of graphene oxide particle size on NF quality at constant PAN and graphene oxide concentrations was examined. After high-power ultrasonication, the size-reduced graphene oxide samples were lyophilized. Appropriate amounts of graphene oxide were redispersed in DMF, and PAN was added and

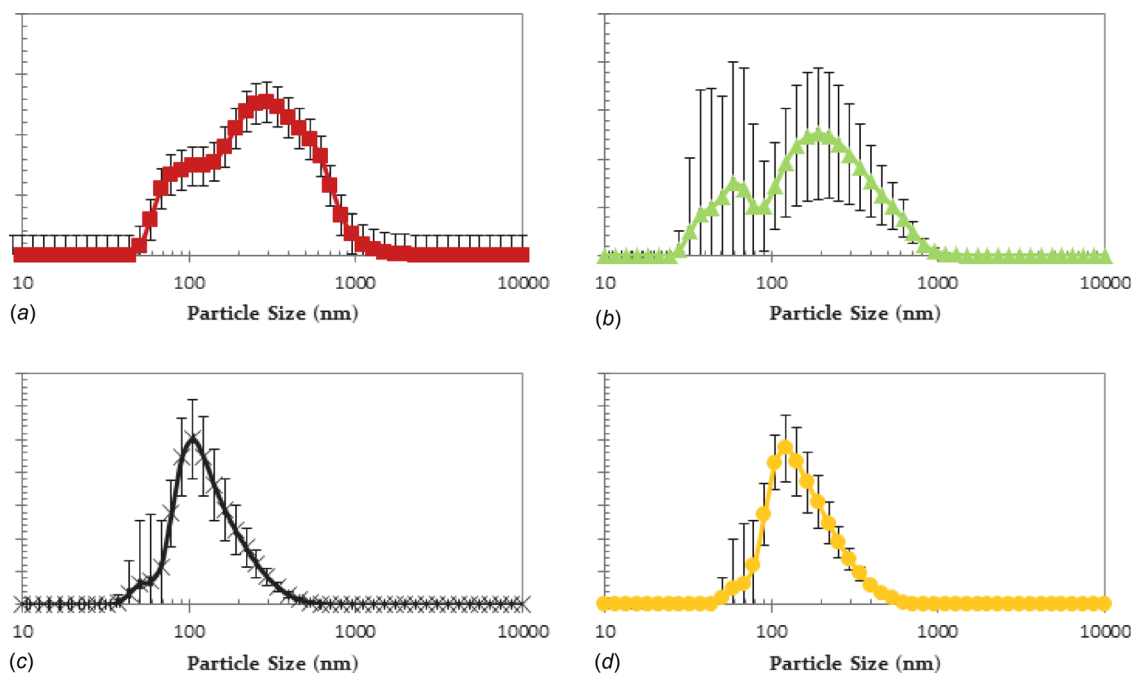


Fig. 1 Particle size of different graphene oxide, sonicated for different lengths of time, as measured by DLS: (a) GO-A (1 h); (b) GO-B (2 h); (c) GO-C (4 h); and (d) GO-nano nonsonicated, produced from nanoscale graphite

dissolved. Nanofibers were electrospun with 1 wt % on PAN (which is smaller than the concentration used in previous work [13]) from 20 cm spinneret–collector distance at 12 kV. The electrospinning was carried out with 10 wt % solids content in DMF. After electrospinning, the different samples were examined in a scanning electron microscope (SEM) for fiber quality (see Fig. 2).

Relatively uniform NFs were produced for all samples. This is different from the previous work where significant nonuniformities were observed in the NFs [13]. Better nanofiber quality in this work might be explained by better control over graphene oxide concentration and dispersion in the final electrospinning solution that was achieved by using dried graphene oxide powders as opposed to dispersions used previously. Multiple samples were examined. Overall, GO-C and GO-nano resulted in the best-quality NFs, which may be due to the fact that smaller nanoparticles, from our experience, usually have higher maximum concentration threshold for manufacturability by electrospinning. As a result, GO-C and GO-nano were chosen for further investigation.

Effect of Graphene Oxide Type and Concentration on Nanofiber Morphology. The GO-C and GO-nano samples mentioned previously had similar particle size distributions, as well as the smallest average particle size among the tested samples. However, they were produced from different raw material graphites. Consequently, their particle size was achieved by different routes.

GO-C underwent long ultra-sonication cycle to reduce its size. On the other hand, GO-nano was produced from smaller-sized raw material. As a result, the two graphene oxides may have distinct characteristics in the density and distribution of functional groups, defects, etc. These differences can have an effect on dispersion quality and the interaction between PAN and graphene oxide particles in solutions. These parameters, in turn, will have an impact on NF quality.

Different amounts of GO-C and GO-nano were introduced into PAN solution. The relative amounts of graphene oxide to PAN were 0.5%, 1%, 2%, 3%, 4%, and 5 wt %. The low graphene oxide concentrations (3% and below) were electrospun from 10 wt % solids solution in DMF. The two highest concentrations were electrospun from 8 wt % solids solution in DMF due to viscosity limitations. Other electrospinning parameters were kept as in the section Effect of Graphene Oxide Type on Nanofiber Morphology. Resulting fiber morphology was examined by SEM (see Fig. 3).

The analysis showed that, although some nonuniformities were present, the quality of the fibers (especially for the case of GO-nano) was very good up to 2 wt % graphene oxide to PAN. Higher graphene oxide concentrations, produced from lower solids content in DMF, exhibited thinner and less uniform fibers and showed considerable amount of beading.

Beading is a well-known phenomenon in electrospinning. It is usually associated with capillary jet instabilities. The beading is a result of a complex interplay between solution viscosity, surface

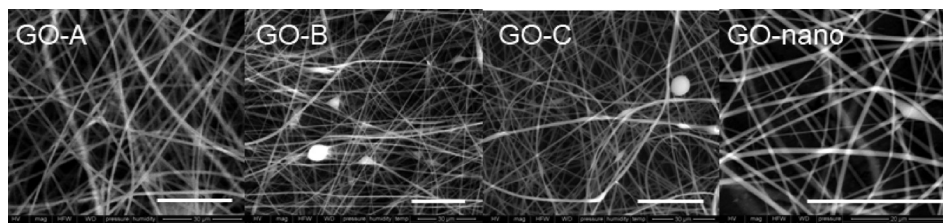


Fig. 2 Effect of graphene oxide particle type on nanofiber morphology at 1 wt % of the polymer. Nanofibers were electrospun from 10 wt % solids solution in DMF from a 20-cm spinneret–collector distance at 12 kV, using a 0.6 ml/h feed rate and 20 ga needle size. Scale bar in all the panels is 30 μ m.

tension, conductivity, and charge density [17]. For example, beading was shown to be suppressed by increased polymer concentration, increased solution conductivity by adding salts, or by increased operating voltage [17–19]. The addition of graphene oxide can further change beading behavior through altering the solution properties and *via* possible bead nucleation effect from nanoparticles. A transmission electron microscope (TEM) investigation in the earlier study [13] showed that NF beads contained large, axially crumpled graphene oxide nanoparticles. The graphene oxides used in this study had smaller average particle sizes. This has likely contributed to better quality and uniformity of the resulting nanofibers. Nevertheless, the infrequent elongated inhomogeneities seen in the NFs with low fractions of graphene oxide could be due to the presence of larger nanoparticles in the samples with relatively broad size distributions (see Fig. 1). Note that the two highest graphene oxide concentrations required lower polymer concentration. This is known to cause more pronounced beading during electrospinning. Consequently, the larger, more spherical beads at higher graphene oxide concentrations are probably the result of classical capillary jet instabilities.

It is important to note that earlier SAED study suggested a global nature of the improvements in the carbon fiber structure as a result of small addition of graphene oxide (see discussion in Ref. [13]). This suggests that slight nanofiber nonuniformity may not be detrimental for CNF structure formation and properties.

Effect of Electrospinning Processing Parameters on Nanofiber Diameter. As mentioned previously, nanofiber diameter critically affects their physical, chemical, electronic, and mechanical properties. It may also be an important geometric scale parameter defining nanofiber applicability in nanotechnological devices and applications. Electrospinning is a complex multiphysics process with multiple factors influencing resulting nanofiber diameters [20–22]. One such factor is the electric field that is usually controlled by varying the applied voltage or the distance between the spinneret and the collector.

There are conflicting reports on the influence of electric field on nanofiber morphology. Yamashita et al. [23], Zhang et al. [18], and Gomes et al. [24] reported an increase in fiber diameter with the increase in electric field. On the other hand, Wang et al. [25]

reported a decrease in fiber diameter as a result of voltage increase in the acceptable voltage range for a given feed rate. Wang and Kumar [26] found that the diameter decreased when the working distance decreased (i.e., the electric field increased), while it remained almost unchanged with changes in voltage. There were also reports of a more complicated relationship [27], where the change in electric field changed not only the average fiber diameter but also the diameter distribution. These reported differences are likely the result of complex influence of the electric field on the development of electrodynamic instabilities that drive jet thinning in the electrospinning process. These instabilities depend on multiple parameters including solution properties as well as minute details of the electric charge and field distributions, in addition to average field strength defined by applied voltage and electrospinning distance. Experiments showed that operating voltage had no major effect on the average diameter of PAN NFs in the range of electrospinning distances and polymer concentrations studied. This is especially true within the context of relatively wide diameter distributions (see Fig. S1 which is available in the [Supplemental Materials](#) on the ASME Digital Collection). On the other hand, generally, smaller spinning distances produced slightly thinner fibers (on average).

Polymer concentration in the fiber spinning solution is known to be one of the most influential parameters determining the final nanofiber diameter. Its influence is often attributed to the variation of solution viscosity with polymer concentration. However, other solution properties, such as surface tension, conductivity, and viscoelasticity, will affect jet elongation and development of electrodynamic jet instabilities that play an important role in fiber formation. Nanofiber formation in electrospinning is also critically affected by fast solvent evaporation from the ultrafine jets [28]. Initial polymer concentration, concentration-dependent mutual diffusivity, and evaporation rate coefficients determine the overall evaporation time as well as the transient polymer concentration profiles [28] that govern solidification. Currently, there is no comprehensive theory to predict the influence of all these complex parameters on the nanofiber diameter. In the absence of such a theory, empirical relationships can be useful to guide process control. Several such relationships were examined, and their applicability for diameter variation prediction was evaluated.

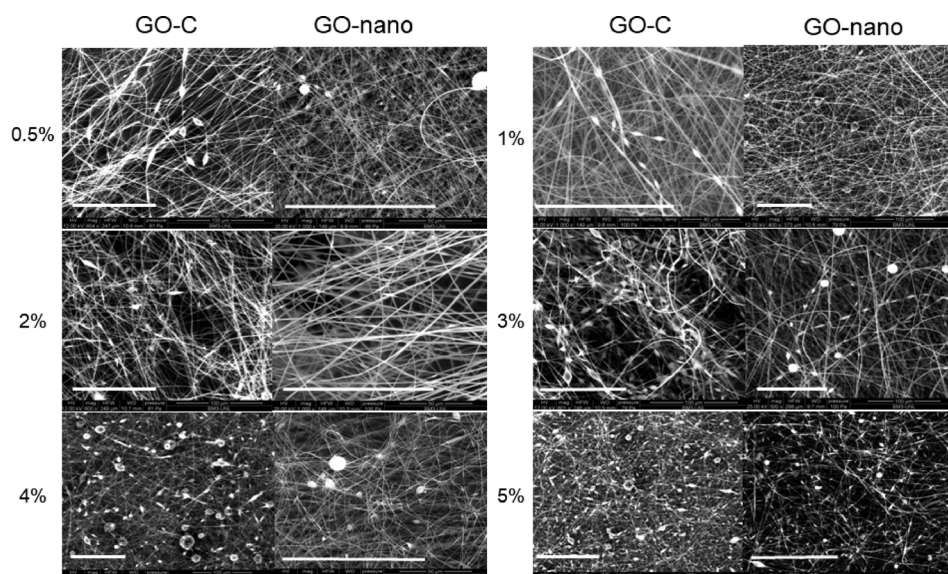


Fig. 3 Electrospun fibers containing different amounts of GO-C and GO-nano. In all samples, graphene oxide concentration was calculated relative to PAN. Samples with 3% and less graphene oxide were electrospun from 10 wt % solids solution in DMF. Samples containing 4% and 5% graphene oxide were electrospun from 8 wt % solids solution of in DMF. Scale bar in all the panels is 100 μm .

NFs were electrospun and examined for several PAN concentrations. NF mats were examined in an SEM. At least five representative images at different locations on the mats were taken. NF diameters were subsequently measured, using IMAGEJ software. For each sample, at least 200 NFs were measured. Uniform fibers were obtained for PAN concentrations of 9 wt % and above. In case of 8% concentration, some beading was observed, but mostly uniform fibers were obtained. 7.5% solution produced more significant beading. In all cases where beading was observed, only uniform nanofiber regions were examined to measure the fiber diameters (see Fig. 5 for the measured average diameters).

In the past, several studies attempted to establish an empirical relationship between the average nanofiber diameter and polymer concentration in electrospinning. Linear relation [29] and power law scaling law (1) [26,30,31] were applied.

$$D = D_0 \left(\frac{C}{C^*} \right)^\alpha \quad (1)$$

An exponential relation between the NF diameter and polymer concentration (2) is another possible functional relation that can be applied

$$D = D_0 * \exp \left\{ \frac{C}{C^*} \right\} \quad (2)$$

Although this model cannot be extended to 0% concentration, it is well known (as discussed previously) that the electrospinning process does not produce fibers at concentrations below certain minimum concentration threshold. The exponential model (2) has an advantage over the power law model (1) as it has only two fitting parameters. Both of these parameters can be extracted from linear regression analysis while only a combination of parameters can be extracted for the three-parameter power law model.

As mentioned previously, in the literature, the linear and the power law models were used to fit variations of the average diameter only. However, for a proper statistical analysis, the NF

diameter distribution should be taken into account. Some key aspects allowing predictions (such as confidence intervals) based on statistical modeling include the assumption of normality of the residuals resulting from the model fit and of constant error variance.

The normality of residuals can be examined in one of two ways. The first method involves comparison of a histogram of residuals to a normal distribution. The second method involves examining the so-called QQ plot. In this plot, quantiles of the data are plotted against quantiles of a normal distribution, with a straight line representing perfect correlation. Deviations from straight line are usual for low and high quantiles (especially for small sample sizes). However, large deviations for large sample sizes indicate significant violation of the normality assumption.

Constant error variance assumption means that the dependent variable (in this case NF diameter) has similar variance for all values of the independent variable (in this case PAN concentration). This assumption is usually examined by plotting the residuals from the fit against the independent variable. If the residuals are randomly distributed, the assumption holds. However, if systematic changes in the distribution of residuals are observed, assumption of constant error variance is violated. To remedy this situation, transformations of the variables (such as power law or natural logarithm) are used.

A linear regression analysis of diameter versus polymer concentration (for the linear model), natural logarithm of diameter versus concentration (for the exponential model) and versus natural logarithm of concentration (for the power law model) was performed in this work. The data were blocked by the day when the tests were carried out (to account for possible changes due to ambient conditions). Diameter measurements for each sample were described as subsampling in the statistical model. Both blocking and subsampling were used as random effects in the statistical model. Statistical analysis was done using SAS[®] Proc Glimmix software, Version 9.2 TS of the SAS System for Windows.

Figures 4(a)–4(c) show the results of the application of the different models. In addition, constant error variance assumption was examined by plotting the residuals versus the predicted diameter

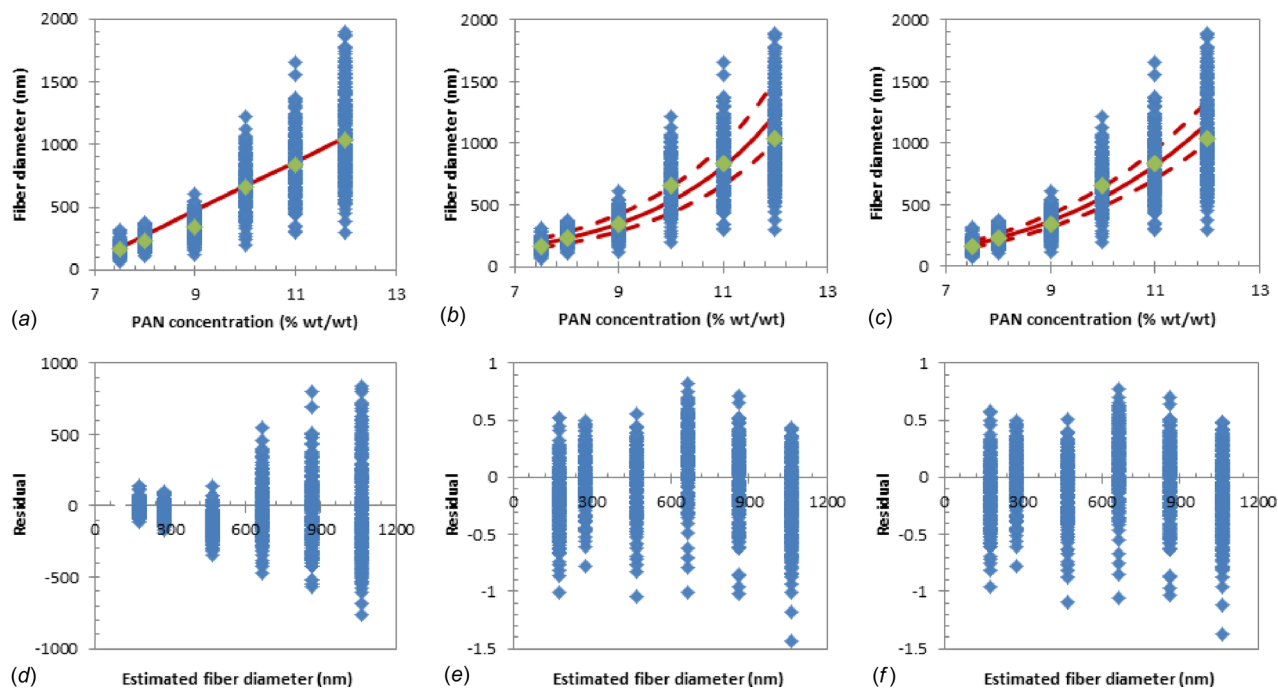


Fig. 4 Fitting the different models. Scatter plot of the data and the linear (a), exponential (b), and power law (c) models. Residuals for the linear (a), exponential (b), and the power law (c) models versus the estimated diameter. The solid lines in (a)–(c) represent the model fit, while the dashed lines in (b) and (c) represent 95% confidence intervals for the fit.

(see Figs. 4(d)–4(f)). As can be seen in Fig. 4(d), the linear model clearly violated the constant error variance assumption. The residuals were also significantly non-normal (see Fig. S2 which is available in the Supplemental Materials on the ASME Digital Collection), indicating that this is not an appropriate model when the whole diameter distributions and not only the average values are taken into account. On the other hand, both the power law and the exponential models showed significantly improved fit. The power law model appears to be slightly better. This fact is also confirmed by lower Akaike information criterion, which indicates better goodness of fit (for both as-spun and carbonized samples). However, the difference is not large. In fact, both models produced very similar predicted diameter values in the examined concentration range with larger departure between models restricted mostly to large diameters (high concentration range). R^2 was 0.71 and 0.73 for the exponential and power models, respectively, while the difference between the two models only exceeded 5.15% of the value predicted by the power law model for 12% PAN. The power law model, though, as mentioned previously, does not allow for a full extraction of the three parameters in the original model, since the transformed model only includes two parameters. Consequently, the exponential model can be considered a good approximation for the examined concentration range (see Table 1 for parameters extracted).

In general, the addition of nanoparticles to electrospinning solutions increases solution viscosity and is therefore usually expected to increase nanofiber diameters. However, incorporation of graphene oxide into the polymer solution can also influence solution conductivity, surface tension, and charge density in the electrospun jets. The complex impact of these parameters can also be system (polymer/solvent) dependent. Indeed, while some studies reported an increase in average fiber diameter as a result of graphene oxide addition [32], others showed that the presence of graphene oxide can actually reduce the fiber diameter [33] or create a bimodal distribution of diameters [34]. We have previously

reported [13] that nanofiber diameters, in fact, decreased in the presence of graphene oxide particles.

The impact of graphene oxide type and size on nanofiber diameters was evaluated by comparing diameter distributions for NFs produced from 1 wt % dispersions of different graphene oxides for a 10 wt % solids content in DMF. In each case, an average and a standard deviation of at least 200 nanofibers was measured and compared to pristine PAN (see Fig. 5(a)). As can be seen, graphene oxides A-C all resulted in larger average diameters than the pristine fibers. The difference was statistically significant from GO-A and GO-C with p -value < 0.0001 . The difference from GO-B was marginally significant with p -value of 0.095. Some decrease in fiber diameter with the decrease in graphene oxide particle size was also observed. As was mentioned previously, all of these graphene oxide types were produced from larger graphite and then sonicated to reduce the particle size. On the other hand, addition of GO-nano resulted in the average diameter smaller than the diameter of pristine fibers. This difference between GO-nano and other graphene oxide particles may be the result of larger density of polar groups on the surface of this graphene oxide type (and subsequently larger charge density). Since the largest density of polar groups after graphite oxidation is on the periphery of the graphene sheets, smaller initial graphite particles would result in larger polar group density in the final graphene oxide. In addition, size reduction achieved by sonication may result in less homogeneous distribution of polar groups.

The effect of graphene oxide concentration on the NF diameter electrospun from 10 wt % solids in DMF was also examined. NFs with GO-nano were used for this purpose. Only concentrations up to 3 wt % graphene oxide relative to PAN were examined (see Fig. 5(b)) since they could be produced from solutions with the same total solids content. Increasing graphene oxide concentration did not permit the use of the same solids content, due to high viscosity. Consequently, a comparison with this concentration would introduce an additional variable impacting NF diameter. In cases

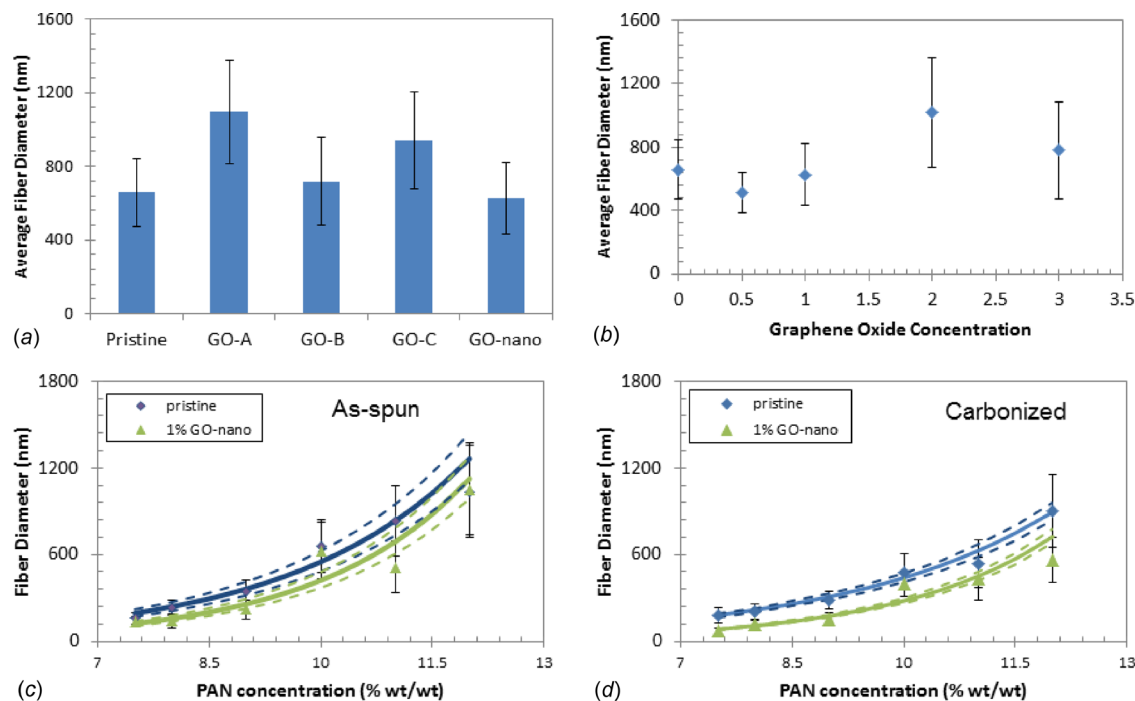


Fig. 5 Effect of graphene oxide on nanofiber diameter. (a) comparison of fiber diameters for pristine and composite nanofibers with 1 wt % of graphene oxide electrospun from 10 wt % solids in DMF; (b) effect of graphene oxide concentration (GO-nano) on composite fiber diameter electrospun from 10 wt % solids in DMF; comparison of fiber diameter for pristine and composite nanofibers containing 1 wt % GO-nano as a function of solids content for as-spun (c); and carbonized at 800 °C (d) samples. The error bars in (c) and (d) are the standard deviations of the sample diameter distribution, the solid lines represent the fit based on the exponential model, and the dashed lines are for the corresponding 95% confidence intervals.

Table 1 Fit parameters for the exponential and the power law models for the pristine and composite, as-spun and carbonized samples

		Exponential model				Power law model			
		D_0	95% CI	C^*	95% CI	$D_0/C^{*\alpha}$	95% CI	α	95% CI
As spun	Pristine	8.54	[7.41;9.84]	2.40	[2.37;2.44]	0.059	[0.051;0.069]	3.99	[3.93;4.05]
	Composite	3.09	[2.68;3.56]	2.03	[2.01;2.06]	0.010	[0.008;0.011]	4.66	[4.60;4.72]
Carbonized	Pristine	12.61	[11.55;13.75]	2.82	[2.77;2.86]	0.194	[0.171;0.221]	3.37	[3.32;3.43]
	Composite	2.43	[2.22;2.66]	2.11	[2.08;2.14]	0.009	[0.008;0.010]	4.53	[4.47;4.59]

where beading was present, only uniform nanofiber regions were measured. As can be seen, fiber diameters decreased for lower graphene oxide concentrations compared to pristine fibers, but for larger concentrations the diameters surpassed the diameters of the pristine sample. This might be the result of either increase in viscosity dominating the system behavior at higher concentrations or better graphene oxide dispersions at lower concentrations (it is significantly harder to disperse the particles well as the viscosity of the system increases).

Finally, the effect of graphene oxide (GO-nano) on fiber diameters at different solids concentrations in solution was also examined, before and after nanofiber carbonization. In addition to the graphene oxide impact on fiber diameter variation, it was also important to determine the range of solids concentrations that produced sufficiently uniform fibers in the presence of graphene oxide. Pristine and templated CNFs were obtained by stabilization and carbonization of electrospun polymer precursors at 800 °C as described in previous studies [13].

Figures 5(c) and 5(d) compare average fiber diameters for pristine and templated (composite) NFs containing 1 wt % GO-nano at different solids contents. The solid lines in the figures correspond to the fit based on the exponential model, and the dashed

lines show the corresponding 95% confidence intervals. Solids content of 7.5 wt % in DMF produced significant beading that was exacerbated by the presence of graphene oxide. While 8 wt % solutions also resulted in some beading, the fibers were more uniform. Starting from 9 wt % solids concentration, uniform nanofibers were obtained. In all cases where beading was present, only uniform regions of the nanofibers were measured.

Comparison of average diameters of the pristine and composite NFs showed that, for the particular system studied, diameters of the composite nanofibers were consistently smaller than for the pristine ones. This effect was preserved during carbonization. The observed difference was found to be statistically significant at the confidence level $\alpha = 0.05$, using both the exponential and the power law models for both as-spun and carbonized samples (see summary of corresponding parameters in Table 1). This result is important since, in addition to the graphitic structure improvement based on the templating effect of graphene oxide, the observed diameter reduction can further increase mechanical properties of the templated CNFs. In addition, there was a statistically significant difference at the same confidence level between the diameters of as-spun and carbonized samples. Diameter distributions after carbonization showed smaller variance (as expressed by

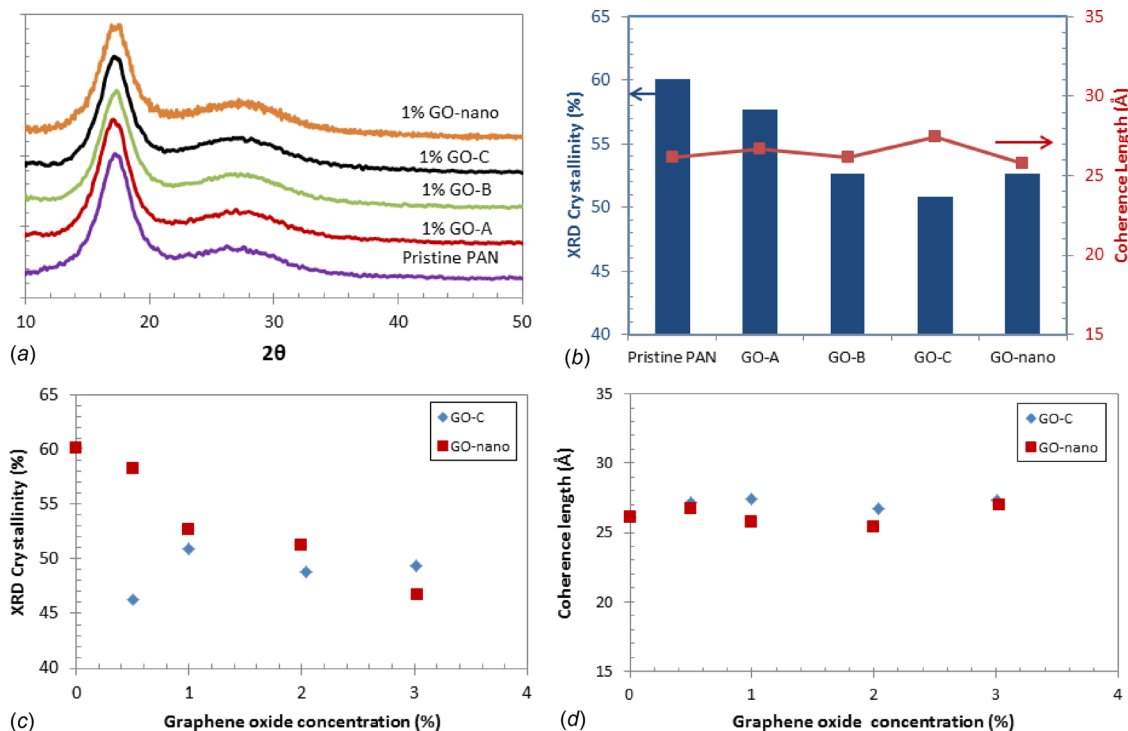


Fig. 6 Effect of graphene oxide on crystal structure of PAN nanofibers electrospun from 10 wt % solids in DMF. (a) XRD diffractograms of pristine PAN and composite nanofibers with different sizes of graphene oxide particles; (b) XRD crystallinity and coherence length extracted from the curves in (a); (c) effect of graphene oxide concentration on crystallinity of PAN nanofibers; and (d) effect of graphene oxide concentration on coherence length in PAN nanofibers.

tighter confidence intervals especially for the larger diameters/higher solids concentrations).

Effect of Graphene Oxide on Polyacrylonitrile Crystallinity and Crystal Structure. Polyacrylonitrile crystallinity may influence carbon structure formation during NF carbonization, as discussed in Refs. [13] and [15]. Crystal structure of the fiber mats was examined by X-ray diffraction. Figure 6(a) shows the comparison of XRD patterns for pristine PAN NFs and the different graphene oxide/PAN composite samples at 1 wt % graphene oxide electrospun from 10 wt % solids after background removal. All samples exhibited a crystalline peak at $2\theta \sim 17.4$ deg and a broad amorphous halo at approximately $2\theta \sim 26.9$ deg, typical of semi-crystalline PAN. The crystalline peak and the amorphous halo were fitted, using Lorentzian curve shapes. XRD crystallinity was extracted by dividing the area under the crystalline peak by the total area under the curve. The coherence length (“crystal size”) was calculated from the width of the main crystalline peak, using the Scherrer equation

$$\text{C.L.}(\text{\AA}) = \frac{K\lambda}{\beta \cos \Theta} = \frac{0.9 * 1.542}{\sqrt{(\text{FWHM}(\text{Rad})^2 - 0.002^2)} \cos \Theta} \quad (3)$$

Shape factor K was taken as 0.9, the λ is the standard wavelength for a copper source, 0.002 was the instrumental peak widening calculated based on a single crystal SI standard, and θ was the Bragg angle for the crystalline peak.

Figure 6(b) shows the comparison of the extracted parameters for different NF samples. As can be seen, coherence length remained small and relatively unchanged compared to pristine PAN NFs. On the other hand, polymer crystallinity decreased in the presence of nanoparticles. The largest decrease of approximately 17% was observed for small graphene oxide particles (GO-C). This decline in crystallinity is consistent with what was observed in our previous studies [13,15] and in other studies such as Chipara et al. [35]. Larger crystallinity decrease for smaller nanoparticles at the same volume fraction of graphene oxide may be the result of more efficient crystal growth inhibition by numerous irregular fine nanoparticles.

Figures 6(c) and 6(d) show the effect of graphene oxide concentration on the crystal parameters of PAN NFs. The XRD examination shown is only for nanofibers with relatively uniform morphology (i.e., concentrations of graphene oxide below 3 wt %). As with the previous results, the coherence length remained relatively unchanged throughout the graphene oxide concentration range, regardless of the graphene oxide type. On the other hand, variation of polymer crystallinity for the samples with two different graphene oxide types was different. Crystallinity steadily declined with the increase in graphene oxide concentration in the GO-nano modified NFs. However, in the NFs modified with the GO-C nanoparticles, crystallinity remained at relatively constant low level, compared to pristine PAN NFs. While this is generally consistent with the above-mentioned hypothesis of crystallization disruption by fine nanoparticles, the difference between the GO-nano and GO-C might be due to the differences in particle size variations as well as the inhomogeneous polar group density in the GO-C, which can also lead to differences in dispersion quality.

Conclusions

The effects of graphene oxide type, size, concentration, and electrospinning processing parameters on graphene oxide/PAN nanofiber morphology were examined. All types of graphene oxide studied produced relatively uniform fibers for 1 wt % graphene oxide concentration. Uniform nanocomposite fibers were produced with up to 2 wt % GO-nano in 10 wt % solid content solutions and with 1% GO-nano relative to PAN electrospun from

solutions with solids content ranging from 9 % to 12 wt % in DMF. The latter processing parameters resulted in good quality nanofibers with controllable average diameters between 250 and 1100 nm for as-spun graphene oxide-modified polymer fibers and from 170 to 750 nm for carbonized NFs. Templated nanofibers with some limited beading inhomogeneities obtained from solutions with 8 wt % solids content had even smaller average fiber diameters of ~ 160 nm for as-spun and ~ 120 nm for carbonized samples. Composite NFs with GO-nano exhibited smaller diameters than the pristine samples throughout the PAN concentration range studied. These results, coupled with the improved graphitic structure after carbonization observed previously [13], can be used for controlled nanofabrication and further informed development of continuous CNFs with improved physical and mechanical properties. Statistical analysis of NF diameter variations taking into account full diameter distributions and performed for the first time for pristine and composite NFs before and after carbonization will provide guidance for future analyses of this important output parameter of the nanomanufacturing process.

Acknowledgment

This work was supported in part by Nebraska Center for Energy Science Research, the grants from National Science Foundation (Division of Material Research-1310534, Civil, Mechanical, and Manufacturing Innovation-1463636), Office of Naval Research (N000141410663).

Funding Data

- Nebraska Center for Energy Science Research, the grants from National Science Foundation (Division of Material Research-1310534; Funder ID: 10.13039/100000078, Civil, Mechanical, and Manufacturing Innovation-1463636; Funder ID: 10.13039/100000147), Office of Naval Research (N000141410663; Funder ID: 10.13039/100000006).

References

- [1] van Noorden, R., 2011, “The Trials of New Carbon,” *Nature*, **469**(7328), pp. 14–16.
- [2] Compton, O. C., and Nguyen, S. T., 2010, “Graphene Oxide, Highly Reduced Graphene Oxide, and Graphene: Versatile Building Blocks for Carbon-Based Materials,” *Small*, **6**(6), pp. 711–723.
- [3] Stankovich, S., Dikin, D. A., Dommett, G. H. B., Kohlhaas, K. M., Zimney, E. J., Stach, E. A., Piner, R. D., Nguyen, S. T., and Ruoff, R. S., 2006, “Graphene-Based Composite Materials,” *Nature*, **442**(7100), pp. 282–286.
- [4] Ramanathan, T., Abdala, A. A., Stankovich, S., Dikin, D. A., Herrera-Alonso, M., Piner, R. D., Adamson, D. H., Schniepp, H. C., Chen, X., Ruoff, R. S., Nguyen, S. T., Aksay, I. A., Prud’Homme, R. K., and Brinson, L. C., 2008, “Functionalized Graphene Sheets for Polymer Nanocomposites,” *Nat Nano*, **3**(6), pp. 327–331.
- [5] Rafiee, M. A., Rafiee, J., Srivastava, I., Wang, Z., Song, H., Yu, Z., and Koratkar, N., 2010, “Fracture and Fatigue in Graphene Nanocomposites,” *Small*, **6**(2), pp. 179–183.
- [6] Potts, J. R., Dreyer, D. R., Bielawski, C. W., and Ruoff, R. S., 2011, “Graphene-Based Polymer Nanocomposites,” *Polymers*, **52**(1), pp. 5–25.
- [7] Rafiee, M. A., Rafiee, J., Wang, Z., Song, H., Yu, Z., and Koratkar, N., 2009, “Enhanced Mechanical Properties of Nanocomposites at Low Graphene Content,” *ACS Nano*, **3**(12), pp. 3884–3890.
- [8] Xu, Z., Sun, H., Zhao, X., and Gao, C., 2013, “Ultrastrong Fibers Assembled From Giant Graphene Oxide Sheets,” *Adv. Mater.*, **25**(2), pp. 188–193.
- [9] Xu, Z., and Gao, C., 2011, “Graphene Chiral Liquid Crystals and Macroscopic Assembled Fibres,” *Nat. Commun.*, **2** p. 571.
- [10] Dong, Z., Jiang, C., Cheng, H., Zhao, Y., Shi, G., Jiang, L., and Qu, L., 2012, “Facile Fabrication of Light, Flexible and Multifunctional Graphene Fibers,” *Adv. Mater.*, **24**(14), pp. 1856–1861.
- [11] Xu, Z., and Gao, C., 2015, “Graphene Fiber: A New Trend in Carbon Fibers,” *Water Today*, **18**(9), pp. 480–492.
- [12] Meng, F., Lu, W., Li, Q., Byun, J.-H., Oh, Y., and Chou, T.-W., 2015, “Graphene-Based Fibers: A Review,” *Adv. Mater.*, **27**(35), pp. 5113–5131.
- [13] Papkov, D., Goponenko, A., Compton, O. C., An, Z., Moravsky, A., Li, X.-Z., Nguyen, S. T., and Dzenis, Y. A., 2013, “Improved Graphitic Structure of Continuous Carbon Nanofibers Via Graphene Oxide Templating,” *Adv. Funct. Mater.*, **23**(46), pp. 5763–5770.

- [14] Dzenis, Y. A., 2004, "Spinning Continuous Fibers for Nanotechnology," *Science*, **304**(5679), pp. 1917–1919.
- [15] Papkov, D., Beese, A. M., Goponenko, A., Zou, Y., Naraghi, M., Espinosa, H. D., Saha, B., Schatz, G. C., Moravsky, A., Loutfy, R., Nguyen, S. T., and Dzenis, Y. A., 2013, "Extraordinary Improvement of the Graphitic Structure of Continuous Carbon Nanofibers Templated With Double Wall Carbon Nanotubes," *ACS Nano*, **7**(1), pp. 126–142.
- [16] Hummers, W. S., and Offeman, R. E., 1958, "Preparation of Graphitic Oxide," *J. Am. Chem. Soc.*, **80**(6), p. 1339.
- [17] Fong, H., Chun, I., and Reneker, D. H., 1999, "Beaded Nanofibers Formed During Electrospinning," *Polymers*, **40**(16), pp. 4585–4592.
- [18] Zhang, D., Karki, A. B., Rutman, D., Young, D. P., Wang, A., Cocke, D., Ho, T. H., and Guo, Z., 2009, "Electrospun Polyacrylonitrile Nanocomposite Fibers Reinforced With Fe₃O₄ Nanoparticles: Fabrication and Property Analysis," *Polymers*, **50**(17), pp. 4189–4198.
- [19] Zong, X. H., Kim, K., Fang, D., Ran, S., Hsiao, B. S., Chu, B., and Hsiao, S. H., 2002, "Structure and Process Relationship of Electrospun Bioabsorbable Nanofiber Membranes," *Polymers*, **43**(16), pp. 4403–4412.
- [20] Reneker, D. H., Yarin, A. L., Zussman, E., and Xu, H., 2007, "Electrospinning of Nanofibers From Polymer Solutions and Melts," *Adv. Appl. Mech.*, **41**, pp. 43–346.
- [21] Reneker, D. H., and Yarin, A. L., 2008, "Electrospinning Jets and Polymer Nanofibers," *Polymers*, **49**(10), pp. 2387–2425.
- [22] Greiner, A., and Wendorff, J. H., 2007, "Electrospinning: A Fascinating Method for the Preparation of Ultrathin Fibers," *Angew. Chem. Int. Ed.*, **46**(30), pp. 5670–5703.
- [23] Yamashita, Y., Aoki, N., Ko, F., and Miyake, H., 2008, "Carbonization Conditions for Electrospun Nanofibre of Polyacrylonitrile Copolymer," *Indian J. Fibre Text. Res.*, **33**, pp. 345–353.
- [24] Gomes, D. S., Da Silva, A. N. R., Morimoto, N. I., Mendes, L. T. F., Furlan, R., and Ramos, I., 2007, "Characterization of an Electrospinning Process Using Different PAN/DMF Concentrations," *Polímeros*, **17**(3), pp. 206–211.
- [25] Wang, C., Chien, H.-S., Hsu, C.-H., Wang, Y.-C., Wang, C.-T., and Lu, H.-A., 2007, "Electrospinning of Polyacrylonitrile Solutions at Elevated Temperatures," *Macromolecules*, **40**(22), pp. 7973–7983.
- [26] Wang, T., and Kumar, S., 2006, "Electrospinning of Polyacrylonitrile Nanofibers," *J. Appl. Polym. Sci.*, **102**(2), pp. 1023–1029.
- [27] Tang, S., Shao, C., Liu, Y., and Mu, R., 2010, "Electrospun Nanofibers of Poly(Acrylonitrile)/Eu³⁺ and Their Photoluminescence Properties," *J. Phys. Chem. Solids*, **71**(3), pp. 273–278.
- [28] Wu, X.-F., Salkovskiy, Y., and Dzenis, Y. A., 2011, "Modeling of Solvent Evaporation From Polymer Jets in Electrospinning," *Appl. Phys. Lett.*, **98**(22), p. 223108.
- [29] He, J.-H., Wan, Y.-Q., and Yu, J.-Y., 2008, "Effect of Concentration on Electrospun Polyacrylonitrile (PAN) Nanofibers," *Fibers Polym.*, **9**(2), pp. 140–142.
- [30] Gupta, P., Elkins, C., Long, T. E., and Wilkes, G. L., 2005, "Electrospinning of Linear Homopolymers of Poly(Methyl Methacrylate): Exploring Relationships Between Fiber Formation, Viscosity, Molecular Weight and Concentration in a Good Solvent," *Polymers*, **46**(13), pp. 4799–4810.
- [31] Arinstein, A., Liu, Y., Rafailovich, M., and Zussman, E., 2011, "Shifting of the Melting Point for Semi-Crystalline Polymer Nanofibers," *EPL*, **93**(4), p. 46001.
- [32] Wan, C., and Chen, B., 2011, "Poly(*ε*-Caprolactone)/Graphene Oxide Biocomposites: Mechanical Properties and Bioactivity," *Biomed. Mater.*, **6**(5), p. 055010.
- [33] Yoon, O. J., Jung, C. Y., Sohn, I. Y., Kim, H. J., Hong, B., Jhon, M. S., and Lee, N.-E., 2011, "Nanocomposite Nanofibers of Poly(D, L-Lactic-Co-Glycolic Acid) and Graphene Oxide Nanosheets," *Compos. Part A Appl. Sci. Manuf.*, **42**(12), pp. 1978–1984.
- [34] Pant, H. R., Park, C. H., Tijing, L. D., Amarjargal, A., Lee, D.-H., and Kim, C. S., 2012, "Bimodal Fiber Diameter Distributed Graphene Oxide/Nylon-6 Composite Nanofibrous Mats Via Electrospinning," *Colloids Surf. A Physicochem. Eng. Asp.*, **407**, pp. 121–125.
- [35] Chipara, M., Cruz, J., Vega, E. R., Alarcon, J., Mion, T., Chipara, D. M., Ibrahim, E., Tidrow, S. C., and Hui, D., 2012, "Polyvinylchloride-Single-Walled Carbon Nanotube Composites: Thermal and Spectroscopic Properties," *J. Nanomater.*, **2012**, p. 435412.